Anisotropic magnetism in $PrCrSb_3$: Bulk properties of single crystals

Manjusha Inamdar, A. Thamizhavel, and S. Ramakrishnan
Tata Institute of Fundamental Research, Mumbai-400005, India
(Received 23 February 2008; published 23 April 2008)

We report anisotropic dc magnetic susceptibility $\chi(T)$, isothermal magnetization $M(H)$, electrical resistivity $\rho(T)$, and heat capacity $C(T)$ measurements on a single crystalline sample of $PrCrSb_3$. The crystal exhibits ferromagnetic ordering below $T_C=112$ K due to ordering of Cr spins. The ferromagnetic phase is highly anisotropic. The anisotropy becomes even more evident at low temperatures at which the rare-earth ion gets magnetically ordered. Pr moments antiferromagnetically order at $T_N=12$ K. The magnetic interplay between these two species (Cr^{3+} and Pr^{3+} ions) gives $PrCrSb_3$ a complex magnetic phase diagram.

DOI: 10.1103/PhysRevB.77.132410 PACS number(s): 75.30.Cr, 71.20.Eh, 75.30.Gw, 75.50.Cc

I. INTRODUCTION

$RCrSb_3$ forms an interesting magnetic system that crystallizes in orthorhombic structure (space group *Pbcm*).[1–5] The crystal structure, as shown in Fig. 1 consists of sheets of Sb atoms arranged on the *b*-*c* plane. The rare-earth ions are placed below and above these Sb sheets in a checkerboard pattern. Each Cr ion is surrounded by six Sb atoms, forming a face (edge) sharing octahedron along the $c(b)$ axis. In short, it is a quasi-two-dimensional structure with RSb and $CrSb_2$ layers stacked along the *a* axis. This layered system displays a variety of magnetic effects due to the interplay between Cr 3*d* electrons and rare-earth 4*f* electrons. Many members of this series are well studied. $LaCrSb_3$, the first member of the series, has a rich magnetic phase diagram.[6] It was conjectured that both itinerant and local moments of Cr are involved in ferromagnetic and antiferromagnetic (AFM) orderings, respectively, in the same compound.[7] $LaCrSb_3$ undergoes a ferromagnetic ordering at 123 K due to ordering of itinerant moments of Cr ion. Also, along the *c* axis, the local moments of Cr antiferromagnetically order at 96 K. This antiferromagnetic transition gets suppressed with an application of moderate magnetic fields. Recent studies[8–11] showed that other members such as $CeCrSb_3$, $SmCrSb_3$, and $GdCrSb_3$ display interesting an interplay of Cr and rare-earth moments. A brief account of the magnetization studies was recently reported by Jackson and Fisk.[10] In this work, we provide a comprehensive study of bulk properties of a high quality single crystals of $PrCrSb_3$, which exhibits a rich magnetic phase diagram due to the interaction of Cr and Pr moments.

II. EXPERIMENTAL DETAILS

Single crystals of $PrCrSb_3$ were grown by a self-flux method. The starting materials of 3*N* pure rare-earth and Cr and 5*N* pure Sb were taken in an off-stoichiometric composition with Pr, Cr, and Sb metals in the ratio of 1:2:20. The metals were placed in a high quality recrystallized alumina crucible and subsequently sealed in a quartz ampoule. The quartz ampoule was heated to 1050 °C and held there for two days in order to achieve proper homogenization of the melt. After homogenization, the ampoule was slowly cooled down to 650 °C, just above the melting point of Sb, then brought down to room temperature at a faster rate. The single crystals present in the solidified Sb flux matrix were removed by means of centrifuging. The phase of the sample was confirmed by performing powder x-ray diffraction on a few grounded single crystals. The Rietveld refinement of the x-ray pattern resulted in the orthorhombic lattice constants $a=13.011(9)$ Å, $b=6.169(7)$ Å, and $c=6.063(1)$ Å with the reliability parameters $R_B=11\%$ and R_F factor=7.03%. From Laue back scattering pictures, the largest surface was found to be perpendicular to the *a* axis. The crystal structure is shown in Fig. 1. The high quality of the crystal was ascertained by the sharp Laue reflection and the energy dispersive x-ray analysis.

The structure shown by Fig. 1 provides the cause for the observed anisotropy in bulk properties and Cr ions seem to be in the trivalent state from the bond length considerations while the rare-earth ions adopt the natural trivalent state except Yb[2]. The temperature dependence of the magnetic susceptibility $\chi(T)$ along the individual axis (*a*, *b*, and *c*) was measured by using a commercial superconducting quantum interference device magnetometer (MPMS5, Quantum Design). The resistivity $\rho(T)$ between 1.5 and 300 K was measured by using an LR700 resistance bridge (Linear Research) by the four-probe method with the contacts made by using silver paste. The in field and zero field heat capacity $C(T)$ between 5 and 200 K was measured by using the commercial Physical Property Measurement System (Quantum Design).

III. RESULTS AND DISCUSSION

Here, we will first discuss the results from our magnetic measurements. Figure 2 shows the anisotropic dc susceptibility $[\chi(T)]$ measurements along the *a*, *b*, and *c* axes for an applied field of 0.1 T.

The susceptibilities along all axes show a sharp anomaly at $T_C=112$ K. This anomaly is attributed to ferromagnetic ordering of Cr moments as also seen in $LaCrSb_3$ at 123 K. The anisotropy in the magnetic properties of this system is evident as we see that the value of χ is much higher along the *b* axis as compared to those along the other two axes. The ratio χ_b/χ_a is almost 1.2 and χ_b/χ_c is 27 below 5 K, giving the measure of anisotropy in the system. The values of χ suggest that *b* is an easy axis for Cr moment ordering. Below T_C, the magnetic phase diagram seems complicated. The

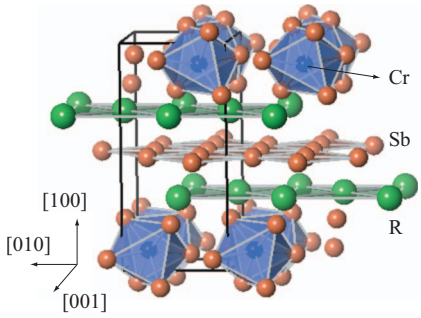

FIG. 1. (Color) The crystal structure of $R\mathrm{CrSb}_3$ consists of 4 f.u. with 20 atoms in the unit cell. The unit cell has a single site for R atoms with position symmetries of 0.308, 0.0024, and 0.25. Three types of Sb atoms with position symmetries: 0.0628, 0.1064, and 0.2500; 0.2159, 0.4989, and 0.2500; and 0.5011, 0.2500, and 0.0000; one type Cr atom with the position symmetry of 0.9095, 0.2500, and 0.0000.

magnetization immediately falls after T_C along the a and c axes. The Pr moments play a role here that antiferromagnetically couple with the Cr moments. At further lower temperatures, magnetization starts to increase until we see a sharp drop in $\chi(T)$ at $T_N=12$ K along all axes attributed to antiferromagnetic ordering of Pr moments. Thus, there is a dip in the susceptibility appearing between the two ordering temperatures T_C and T_N as a result of Pr^{3+} and Cr^{3+} interaction. The inset of Fig. 2 shows the high temperature inverse magnetic susceptibility along all axes fitted to the modified Curie–Weiss expression, $\chi=\chi_0+C/T-\theta$. The value of χ_0 is 4×10^{-3} emu/mol. The Curie constant gives an effective moment of $4.24\mu_B$ as compared to $3.01\mu_B$ for LaCrSb_3. The value of θ is positive, as expected for ferromagnets, and is about 130 K along all of the axes.

Figure 3 shows the evolution of the dip feature with an applied field for the b axis. The dip becomes shallower with

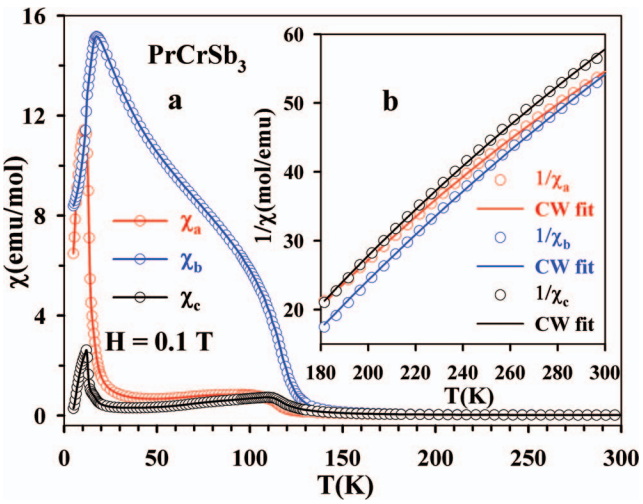

FIG. 2. (Color) (a) Shows the susceptibility $[\chi(T)]$ for all of the axes for PrCrSb_3 down to 2 K from room temperature at 0.1 T of field. The lines shown in the main panel are only a guide for the eyes. The inset (b) shows the high temperature inverse susceptibility for all axes fitted to the modified Curie–Weiss expression; the solid lines are the fits and the open circles are the actual data points.

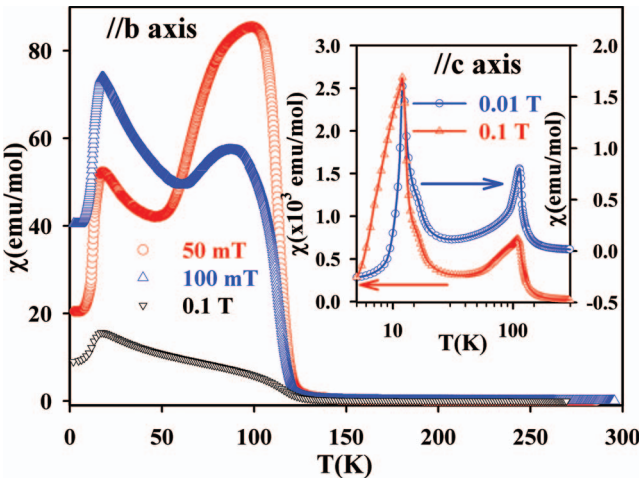

FIG. 3. (Color) Temperature dependence of the susceptibility at 50 mT, 100 mT, and 0.1 T along the b axis for PrCrSb_3. The inset shows the temperature dependence of the susceptibility (χ_c) at 100 mT and 0.1 T along the c axis. Note the negative value for χ_c (Y1 axis) at 10 mT at low temperatures.

higher fields and finally disappears at 0.1 T. This observation supports our claim that there is some compensation of Cr moments from Pr occurring below T_C bringing $\chi(T)$ down. As we increase the field, Pr moments flip in the direction of Cr moments, resulting in vanishing of the dip feature. The disappearance also tells that b is an easy axis for Cr moment ordering, as said before. The inset of Fig. 3 shows an interesting feature that is the compensation of bulk magnetization achieved at low fields. It is interesting to note that the susceptibility value along the c axis could even become negative at low temperatures for a field below 10 mT. Clearly, the Cr and Pr spins are antiparallel aligned to give this compensation and the large contribution of conduction electron spin polarization lifts the magnetization value above zero at 0.1 T as compared to the data at 0.01 T shown in the inset of Fig. 3. For further understanding of magnetic properties of PrCrSb_3, we have performed the isothermal magnetization measurements on the sample along all of the three axes at temperatures of 2, 10, and 50 K.

For all of the temperatures along the a, b, and c axes, the magnetization appears hysteretic. As seen in Fig. 4, the magnetization along the a and b axes saturates to $3.63\mu_B$ and $3.75\mu_B$, respectively, as compared to the saturation moment of $1.5\mu_B$ for LaCrSb_3. The saturation moment has contributions both from Pr^{3+} and Cr^{3+} ions. The moments along the c axis do not saturate until 12 T of field. The high value of moments along a suggests that a is an easy axis for Pr moments. We also see a field induced crossover for Pr easy axis from the a to the b axis at 6 T. Clearly from our magnetic susceptibility and isothermal magnetization measurements, we can say that PrCrSb_3 is ferromagnetic at all temperatures below T_C with the presence of overriding AFM due to ordering of Pr moments, giving the system a complicated magnetic phase diagram. The ordering temperatures observed here are much lower compared to the polycrystalline report on this sample,[5] where $T_C=147$ K and $T_N=17$ K.

The resistivity $\rho(T)$ versus temperature data for the sample is shown in Fig. 5 for temperatures between 1.5 and

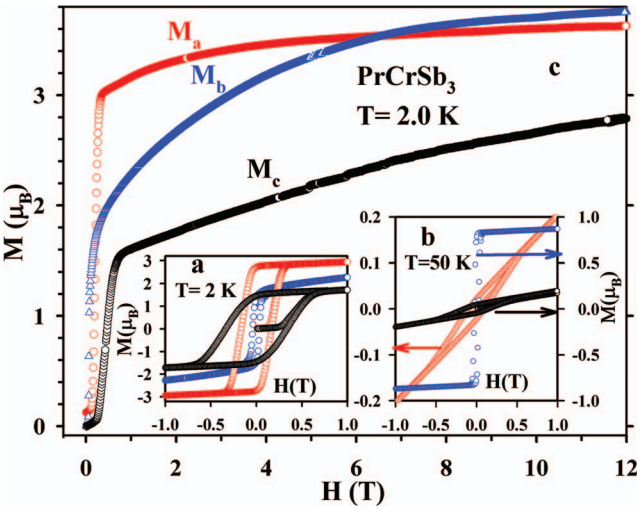

FIG. 4. (Color) Magnetization versus field $\chi(H)$ (presence of field in the forward cycle) for $PrCrSb_3$ along the a, b, and c axes. We see here the easy axis of magnetization orienting from a to b at 6 T of field. The inset (a) shows the ferromagnetic hysteresis at 2 K, while the inset (b) exhibits the hysteresis due to ferromagnetic ordering Cr moments at 50 K with the easy axis of magnetization along the b axis. The main panel (c) displays the magnetization data up to 12 T at 2.0 K.

300 K for an excitation current I along individual axes. As expected, the sample shows a sharp fall in $\rho(T)$ below T_C due to the decrease in the spin-disorder scattering at ferromagnetic transition. The sample thickness was too small along the c axis, so the resistive measurement along this axis was difficult and is not reported here. The sample exhibits high anisotropy in resistivity with room temperature values of $\rho_a(300\ \mathrm{K})=903\ \mu\Omega\ \mathrm{cm}$, $\rho_b(300\ \mathrm{K})=148\ \mu\Omega\ \mathrm{cm}$, and $\rho_c(300\ \mathrm{K})=106\ \mu\Omega\ \mathrm{cm}$ for $PrCrSb_3$.

The observed anisotropy is comparable to that observed in other $RCrSb_3$ crystals. We also see a low temperature

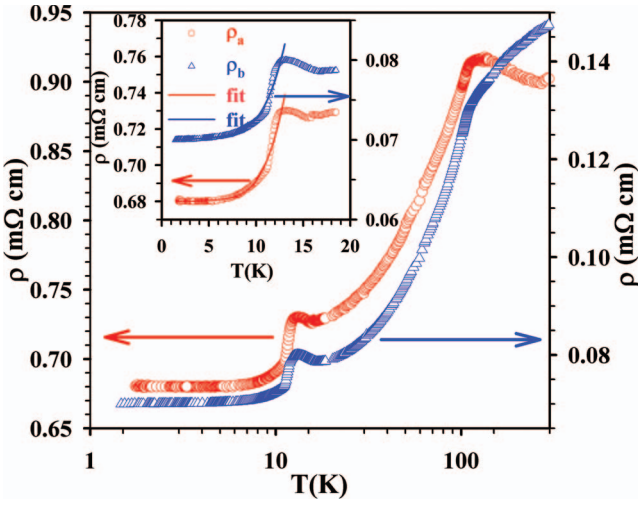

FIG. 5. (Color) Top panel shows the resistivity ρ versus temperature T data for the $PrCrSb_3$ system with a current I along the a and b axes. The inset shows the resistivity along the a and b axes at low temperatures. The solid lines in the inset are fits to the data (see text).

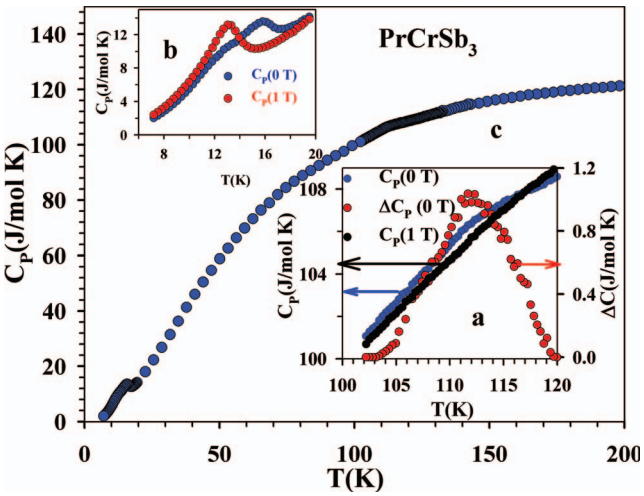

FIG. 6. (Color) Specific heat versus temperature for the $PrCrSb_3$ sample. We see two well-defined kinks in the data at T_C and T_N. The inset (a) shows the C_P data at high temperatures (Y axis) and the change in the heat capacity due to ferromagnetic ordering of Cr spins by subtracting the lattice contribution to the heat capacity. The smearing of the heat capacity anomaly under a magnetic field of 1 T is also shown in the inset (a). The inset (b) shows the heat capacity data under 0 and 1 T with the anomaly due to magnetic ordering of Pr ions. The main panel (c) shows the overall temperature dependence of the heat capacity from 6 to 200 K.

anomaly in the resistivity data along the a and b axes at $T_N=12$ K. This sharp fall in $\rho(T)$ at T_N can also be explained by a decrease in the spin-disorder scattering due to magnetic transition. The inset that shows the dependence of resistivity at low temperatures is fitted to the expression

$$\rho(T) = \rho_0 + aT^2 + bT\Delta[1 + 2T/\Delta]\exp(-\Delta/T), \qquad (1)$$

where ρ_0 is the residual resistivity, a is a coefficient responsible for electron-electron scattering, b is the coefficient responsible for electron-magnon scattering, and Δ is the gap in the spin-wave spectrum for the ferromagnet. Since the sample is in the ferrimagnetic state even at low temperatures, we believe that one can use Eq. (1) to analyze the data below T_N. The parameters obtained from the fit for ρ_a are $\rho_0=680\ \mu\Omega\ \mathrm{cm}$, $a=0.03\ \mu\Omega\ \mathrm{cm/K^2}$, $b=6.2$, and $\Delta=64$ K, whereas the parameters obtained for the fit for ρ_b are $\rho_0=70\ \mu\Omega\ \mathrm{cm}$, $a=0.011\ \mu\Omega\ \mathrm{cm/K^2}$, $b=1.23$, and $\Delta=64.5$ K. It is important to note that the values of the spin-wave gap obtained are almost the same for both axes (even though the anisotropy factor is nearly 10), which gives credibility to our idea of using Eq. (1) to fit the low temperature resistivity data.

The temperature dependence of the heat capacity $C_P(T)$ of $PrCrSb_3$ between 6 and 200 K is shown in Fig. 6. Unlike $LaCrSb_3$, we see a well-defined peak in the heat capacity data of $PrCrSb_3$ at $T_C=112$ K. The peak at T_C gets smeared with the application of 1 T of field, as seen in inset (a) of Fig. 6. The broadening of the heat capacity peak for $PrCrSb_3$ at T_C is supportive of the fact that Cr moments undergo a ferromagnetic transition. The jump $\Delta C \approx = 1$ J/mol K [shown in inset (a) of Fig. 6] confirms the bulk nature of the

ferromagnetic ordering of Cr moments. We also see the low temperature kink in the heat capacity data at $T_N=12$ K. This peak as seen in Fig. 6(b) gets shifted to a lower value of temperature with an application of field, implying that the magnetic ordering is AFM at this temperature. Unlike other samples, we have not found any published work (prior to this work) on the bulk properties of a single crystal of $PrCrSb_3$.

IV. CONCLUSION

To conclude, we have grown single crystals of the compound $PrCrSb_3$ by flux growth method and characterized them by x-ray, Laue back scattering, dc magnetic susceptibility, isothermal magnetization, resistivity, and heat capacity (0 and 1 T) measurements. All measurements confirm bulk ferromagnetic ordering below 112 K in this compound. The presence of f moments of Pr ion shifts the T_C to a lower value as compared to that of $LaCrSb_3$. The easy axis of magnetization for Cr moments continues to be the b axis as in the case of $LaCrSb_3$ and $CeCrSb_3$. Pr^{3+}-Cr^{3+} interaction gives a complex magnetic phase below T_C. This gives different signatures of $\chi(T)$ along all the three axes. However, unlike $CeCrSb_3$ (Ref. 10) in $PrCrSb_3$, we see a sharp magnetic ordering due to moments of Pr at $T_N=12$ K. The easy axis for magnetization for the AFM ordering is along the a axis and shifts to b at a higher field. The resistivity and heat capacity measurements for $PrCrSb_3$ also show anomaly at these two ordering temperatures, which confirm our analysis of the magnetic properties of this system. The existence of gap in the spin-wave spectrum below the AFM ordering of Pr spins and the magnetic compensation of Cr and Pr spins at low temperatures (even negative susceptibility at 10 mT along c axis) make $PrCrSb_3$ an interesting compound in the family of $RCrSb_3$ series. Neutron scattering studies are underway for detailed understanding of the magnetic phase of this compound.

[1] M. Brylak and W. Jeitschko, Z. Naturforsch., B: Chem. Sci. **50**, 899 (1995).
[2] S. J. Crerar, L. Deakin, and A. Mar, Chem. Mater. **17**, 2780 (2005).
[3] M. J. Ferguson, R. W. Hushagen, and A. Mar, J. Alloys Compd. **249**, 191 (1997).
[4] N. P. Raju, J. E. Greedan, M. J. Ferguson, and A. Mar, Chem. Mater. **10**, 3630 (1998).
[5] M. Leonard, S. Saha, and N. Ali, J. Appl. Phys. **85**, 4759 (1999).
[6] D. D. Jackson, M. Torelli, and Z. Fisk, Phys. Rev. B **65**, 014421 (2001).
[7] E. Granado, H. Martinho, M. S. Sercheli, P. G. Pagliuso, D. D. Jackson, M. Torelli, J. W. Lynn, C. Rettori, Z. Fisk, and S. B. Oseroff, Phys. Rev. Lett. **89**, 107204 (2002).
[8] D. D. Jackson and Z. Fisk, J. Magn. Magn. Mater. **256**, 243 (2004).
[9] D. D. Jackson and Z. Fisk, J. Alloys Compd. **377**, 106 (2003).
[10] D. D. Jackson and Z. Fisk, Phys. Rev. B **73**, 024421 (2006).
[11] D. D. Jackson, S. K. McCall, A. B. Karki, and D. P. Young, Phys. Rev. B **76**, 064408 (2007).